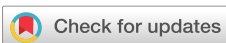


RESEARCH ARTICLE | SEPTEMBER 15 2023

## Multifunctional acoustic devices based on unbalanced gain–loss materials

Zhonghan Fei  ; Jun Lan; Menyang Gong  ; Yun Lai  ; Xiaozhou Liu 

AIP Advances 13, 095016 (2023)

<https://doi.org/10.1063/5.0152600>View  
OnlineExport  
Citation

CrossMark

### Articles You May Be Interested In

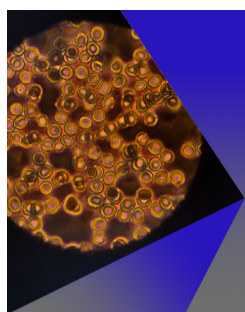
Completing the dark matter solutions in degenerate Kaluza-Klein theory

*J. Math. Phys.* (April 2019)

Gibbs measures based on 1d (an)harmonic oscillators as mean-field limits

*J. Math. Phys.* (April 2018)

An upper diameter bound for compact Ricci solitons with application to the Hitchin–Thorpe inequality. II

*J. Math. Phys.* (April 2018)**AIP Advances**Special Topic: Medical Applications  
of Nanoscience and Nanotechnology

Submit Today!

 AIP  
Publishing

# Multifunctional acoustic devices based on unbalanced gain-loss materials

Cite as: AIP Advances 13, 095016 (2023); doi: 10.1063/5.0152600

Submitted: 6 April 2023 • Accepted: 25 August 2023 •

Published Online: 15 September 2023



View Online



Export Citation



CrossMark

Zhonghan Fei,<sup>1</sup> Jun Lan,<sup>2</sup> Menyang Gong,<sup>1</sup> Yun Lai,<sup>1,a)</sup> and Xiaozhou Liu<sup>1,3,a)</sup>

## AFFILIATIONS

<sup>1</sup> Key Laboratory of Modern Acoustics, Institute of Acoustics and School of Physics, Collaborative Innovation Center of Advanced Microstructures, Nanjing University, Nanjing 210093, China

<sup>2</sup> College of Computer Science and Technology, Nanjing Tech University, Nanjing 211800, China

<sup>3</sup> State Key Laboratory of Acoustics, Institute of Acoustics, Chinese Academy of Sciences, Beijing 100190, China

<sup>a)</sup> Authors to whom correspondence should be addressed: [laiyun@nju.edu.cn](mailto:laiyun@nju.edu.cn) and [xzliu@nju.edu.cn](mailto:xzliu@nju.edu.cn)

## ABSTRACT

The realization of multifunction by simply combining acoustic devices together is always attractive, but it is never an easy task due to the complexity of most acoustic metamaterials. In this paper, a kind of unbalanced gain-loss acoustic metasurface is designed, which can work as an energy amplifier, suggesting that it may be applied to an acoustic signal detector or a sensor. In addition, an acoustic negative refraction system is established by simply putting two of these metasurfaces together, which can produce negative refraction for the acoustic waves from different directions and different incident angles, even focusing and imaging with precisely selected parameters. These functions are quite rare for materials without the double-negative-parameter. This work provides a new route to use the gain/loss materials and achieve multifunctions without complex design.

© 2023 Author(s). All article content, except where otherwise noted, is licensed under a Creative Commons Attribution (CC BY) license (<http://creativecommons.org/licenses/by/4.0/>). <https://doi.org/10.1063/5.0152600>

## I. INTRODUCTION

The control of acoustic wave transmission is always a puzzling problem and challenging project for scientists. The past few decades saw intriguing achievements in acoustic metamaterials, such as double negative materials,<sup>1–3</sup> zero-index metamaterials,<sup>4,5</sup> and acoustic wave clocking,<sup>6,7</sup> providing unprecedented methods to this problem. In recent years, the development of metasurface<sup>8</sup> furnishes more chances on the research of wave manipulation. Metasurface is an expansion of the metamaterial, with well-designed units in subwavelength scale to control the reflection, transmission, and direction of an acoustic wave, for example, the ultrathin Schroeder diffuser,<sup>9</sup> subwavelength acoustic absorber,<sup>10–13</sup> acoustic metalens,<sup>14–16</sup> and coding metasurface.<sup>17–22</sup> Among them, the appliance of gain-loss acoustic metamaterials has been a new approach to manipulate the wave; the elaborately modulated balanced gain-loss acoustic materials are a research focus of parity-time (PT) symmetric acoustics.<sup>23</sup> Although the concept of PT-symmetry was originally introduced from quantum mechanics,<sup>24</sup> several interesting physical properties have been deeply studied in PT-symmetric acoustics. For instance,

the exception point (EP), where the two eigenstates coalesce at the same time, results in many interesting phenomena, such as unidirectional invisibility,<sup>25,26</sup> asymmetric diffraction,<sup>27</sup> and single-side beam splitting,<sup>28</sup> has been realized both in theory and experiment. In optics and electronics, the coherent perfect absorber (CPA)-laser point existing in the broken phase, where the eigenvalues of the scattering matrix of the PT-symmetric system become zero and infinity simultaneously, which correspond to the states of a CPA and laser, respectively, is another research highlight in optics and electronics.<sup>29,30</sup> In acoustics, the system with similar physical properties is called a CPA-sound amplification by stimulated emission of radiation(saser) system,<sup>31,32</sup> corresponding to the concept of CPA-laser, which provides a brand-new way for acoustic wave manipulation and acoustic logic gates and so on. Besides the PT-symmetric system, the conventional metasurface made by unbalanced gain-loss pairs can also cause unconventional physical phenomena. In this work, we design an acoustic amplifier based on a pair of unbalanced gain-loss regions, which does not satisfy the PT-symmetric condition but can also have a saser point. The significant enhancement of the amplitude of the incident acoustic wave can be achieved at the

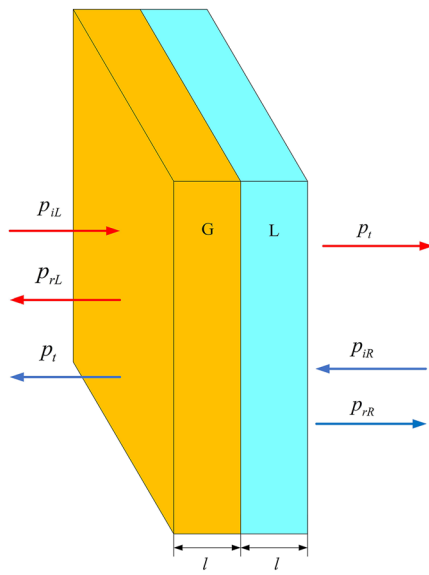


**FIG. 1.** Schematic picture of an unbalanced gain–loss laser system by sticking a gain (G) region and a loss (L) region together. The thickness of each layer is 25 mm.  $p_{iL(R)}$ ,  $p_{rL(R)}$ , and  $p_i$  denote the sound pressure of incident wave, reflected wave from left (right), and transmitted wave, respectively.

saser point for a specific frequency, which means a great potential to be a great signal detector and a hypersensitive sensor. Based on this system, we propose a double unbalanced negative refractive system realized by two parallel metasurfaces. We also find the designed system can work as a metalens based on our research, having good focusing and imaging capability if designed carefully.

## II. RESULTS

### A. Properties of one single unbalanced gain–loss saser system

As shown in Fig. 1, the unbalanced gain–loss saser system is composed of a gain (G) region and loss (L) region, each of them with thickness  $l = 25$  mm. The background medium is air, whose density and wave velocity are  $\rho_0 = 1.21 \text{ kg/m}^3$  and  $c_0 = 343 \text{ m/s}$ , respectively. The density of both the gain and loss regions is  $\rho_{G(L)} = 1.21 \text{ kg/m}^3$ , equal to the density of air, and refractive indices for the gain and loss region are  $n_G = c_0/c_G = 1 + 0.73i$  and  $n_L = c_0/c_L = 1 - 0.12i$ , respectively.  $c_G$  is the sound velocity in the gain region and  $c_L$  denotes the sound velocity in the loss region. Unlike the PT-symmetric system,<sup>23</sup> the absolute values of the imaginary part of the refractive indices are not equal. To derive the transmission/reflection coefficient and the sound pressure distribution in the system, the transfer matrix method (TMM)<sup>33</sup> is applied (see the

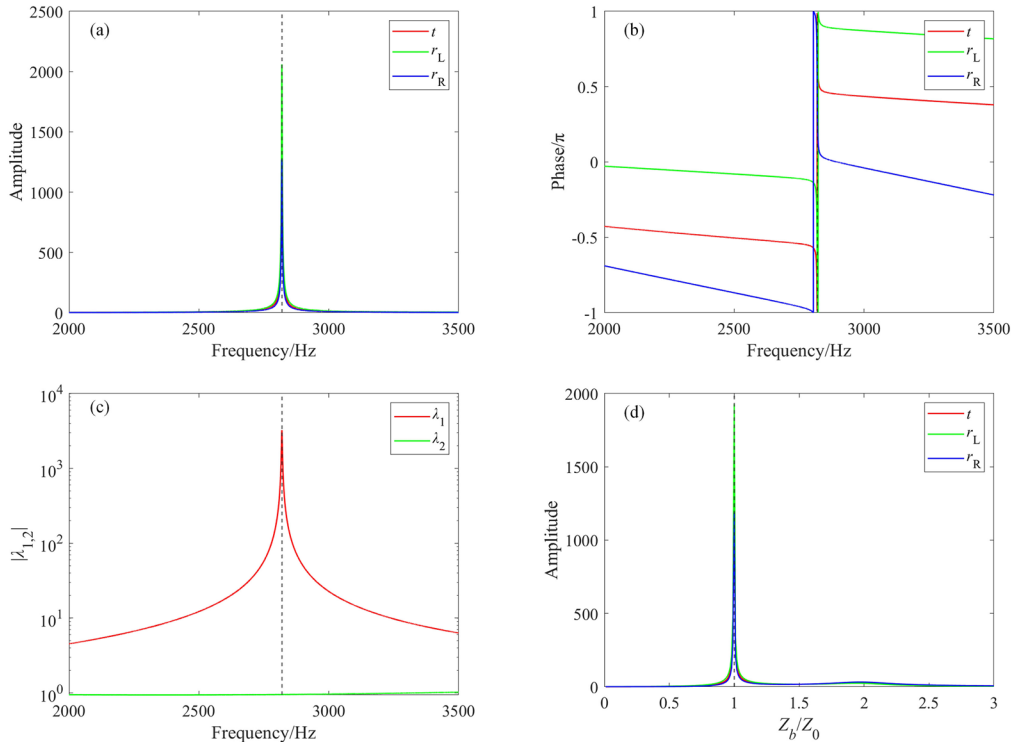


**FIG. 2.** (a) The amplitudes and (b) phases of the transmission, left-reflection, and right-reflection coefficients of the unbalanced gain–loss system with the variation of frequency. (c) The absolute values of the eigenvalues of the scattering matrix of this acoustic system with the variation of frequency. (d) The amplitude of the transmission, left-reflection, and right-reflection coefficients of the system vs the characteristic impedance of the background medium (normalized by the air characteristic impedance already) at 2820 Hz.

[Appendix](#) for the detailed derivation). When a plane wave propagates through the whole composite structure, it can be expressed as

$$P_O = \begin{pmatrix} p_t \\ 0 \end{pmatrix} = T \cdot \begin{pmatrix} p_i \\ p_r \end{pmatrix} = T \cdot P_{in}, \quad (1)$$

$$T = \begin{pmatrix} T_{11} & T_{12} \\ T_{21} & T_{22} \end{pmatrix}, \quad (2)$$

where  $p_i$ ,  $p_r$ , and  $p_t$  are the sound pressure of incident, reflected, and transmitted waves, and  $P_{in}$  and  $P_O$  denote the state vectors of sound pressure distribution of the incidence and transmission side, respectively. It is noteworthy that the determinant of the total transfer matrix  $T$  is always one. Therefore, the reflection coefficient and transmission coefficient can be derived as  $r_L = \frac{p_L}{p_i} = -\frac{T_{21}}{T_{22}}$ ,  $r_R = \frac{p_R}{p_R} = \frac{T_{12}}{T_{22}}$ ,  $t = \frac{p_t}{p_i} = \frac{T_{11}T_{22} - T_{12}T_{21}}{T_{22}} = \frac{1}{T_{22}}$ , where  $r_{L(R)}$  denotes the reflection coefficient for the wave incident from left(right) and  $t$  is the transmission coefficient.

Based on all the studies above, we calculate the amplitude and phase of the transmitted and right (left) reflected waves and depict them in [Figs. 2\(a\)](#) and [2\(b\)](#), which shows that the amplitudes of the transmission, left-reflection, and right-reflection coefficients all become extremely large values and that means the unbalanced gain-loss metasurface has a saser effect at the frequency of 2820 Hz, and there is a  $\pi$  phase jump for all of them at this frequency as well. The existence of the poles means that the  $T_{22}$  in the transfer matrix  $T$  is zero; thus, the matrix can be revised as  $T = \begin{pmatrix} T_{11} & T_{12} \\ 0 & 0 \end{pmatrix}$  at the frequency of 2820 Hz. Moreover, we define the scattering matrix

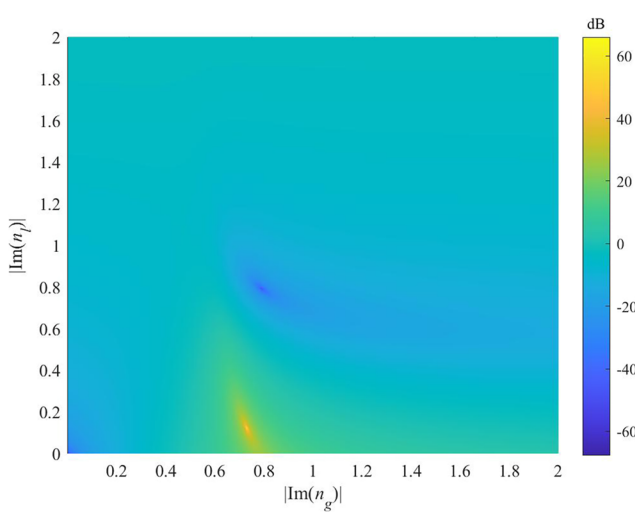


**FIG. 3.** The amplitude of the right-reflection coefficient with different values of the imaginary parts of the refractive indices of the gain and loss materials at the frequency of 2820 Hz. The maximum point and zero point indicate the saser point and exceptional point of the system, respectively. The unit has been converted to decibels.

$S = \begin{pmatrix} t & r_L \\ r_R & t \end{pmatrix}$  to study the system further. The eigenvalues of the scattering matrix are derived as  $\lambda_{1,2} = t \pm \sqrt{r_L r_R}$ . As shown in [Fig. 2\(c\)](#), the absolute value of one of the eigenvalue  $|\lambda_1|$  comes to infinity and the other one  $|\lambda_2| < 1$  at 2820 Hz, which also indicates saser point at this frequency. We also study the influence of the background medium around on the system, and the result is shown in [Fig. 2\(d\)](#). It is shown that when the background medium is air, the saser point occurs even when the frequency of the incident wave is at its operating frequency  $f = 2820$  Hz. These physical properties show the potential of the system to be a specific-frequency sound energy amplifier or an acoustic signal detector or a sensor to detect the slight change in the surrounding medium under different circumstances. In [Fig. 3](#), we present the amplitude of reflection coefficient (in dB) for the right-incident wave as a function of varying imaginary parts of the gain (loss) materials, indicating that the saser point of this metasurface only achieves when the refractive indices of the materials set just at those points, and the system needs to be carefully designed in view of this. The zero point on this picture indicates the EP point of the PT-symmetric system with the same geometric design of the unbalanced gain-loss system, which has been studied in previous studies.<sup>23,25–28</sup>

## B. Design of the unbalanced gain-loss negative refraction system

### 1. Negative refraction

The unbalanced gain-loss negative refraction system (UGNRS) is designed with two same gain-loss regions that have been investigated before. As shown in [Fig. 4\(a\)](#), these two regions are parallel to each other and separated by the air region with thickness  $d$ . By using the TMM, we can also calculate the properties of the whole negative refraction system. At the saser point, the transfer matrix of the UGNRS based on Eqs. (1) and (2) can be expressed as

$$T_{UGNRS} = T \begin{pmatrix} e^{-jk_0 d} & 0 \\ 0 & e^{jk_0 d} \end{pmatrix} T = \begin{pmatrix} T_{11}^2 e^{-jk_0 d} - e^{jk_0 d} & T_{11} T_{12} e^{-jk_0 d} \\ -\frac{T_{11} e^{-jk_0 d}}{T_{12}} & -e^{-jk_0 d} \end{pmatrix}, \quad (3)$$

$$t_{UGNRS} = -e^{jk_0 d}, r_{UGNRSL} = -\frac{T_{11}}{T_{12}}, r_{UGNRSR} = -T_{11} T_{12}, \quad (4)$$

where  $t_{UGNRS}$ ,  $r_{UGNRSL}$ , and  $r_{UGNRSR}$  are the transmission, left-reflection, and right-reflection coefficients, respectively. The amplitudes and phases of transmission, left-reflection, and right-reflection coefficients of the UGNRS with normally incident wave at 2820 Hz are shown in [Figs. 4\(b\)](#) and [4\(c\)](#), which can be seen that at the saser point of one single system, the amplitudes of transmission and reflection coefficients of the UGNRS are all constants, regardless of the distance  $d$ . In particular, the amplitude of transmission coefficient  $|t| = 1$  and the phase of reflection coefficients are irrelevant with the distance between the two metasurfaces. Moreover, the wave propagation in the middle region between the two parallel metasurfaces deserves research as well. The state vectors  $P_{mL}$  and  $P_{mR}$ , which denote the sound pressure distribution in the middle region with the

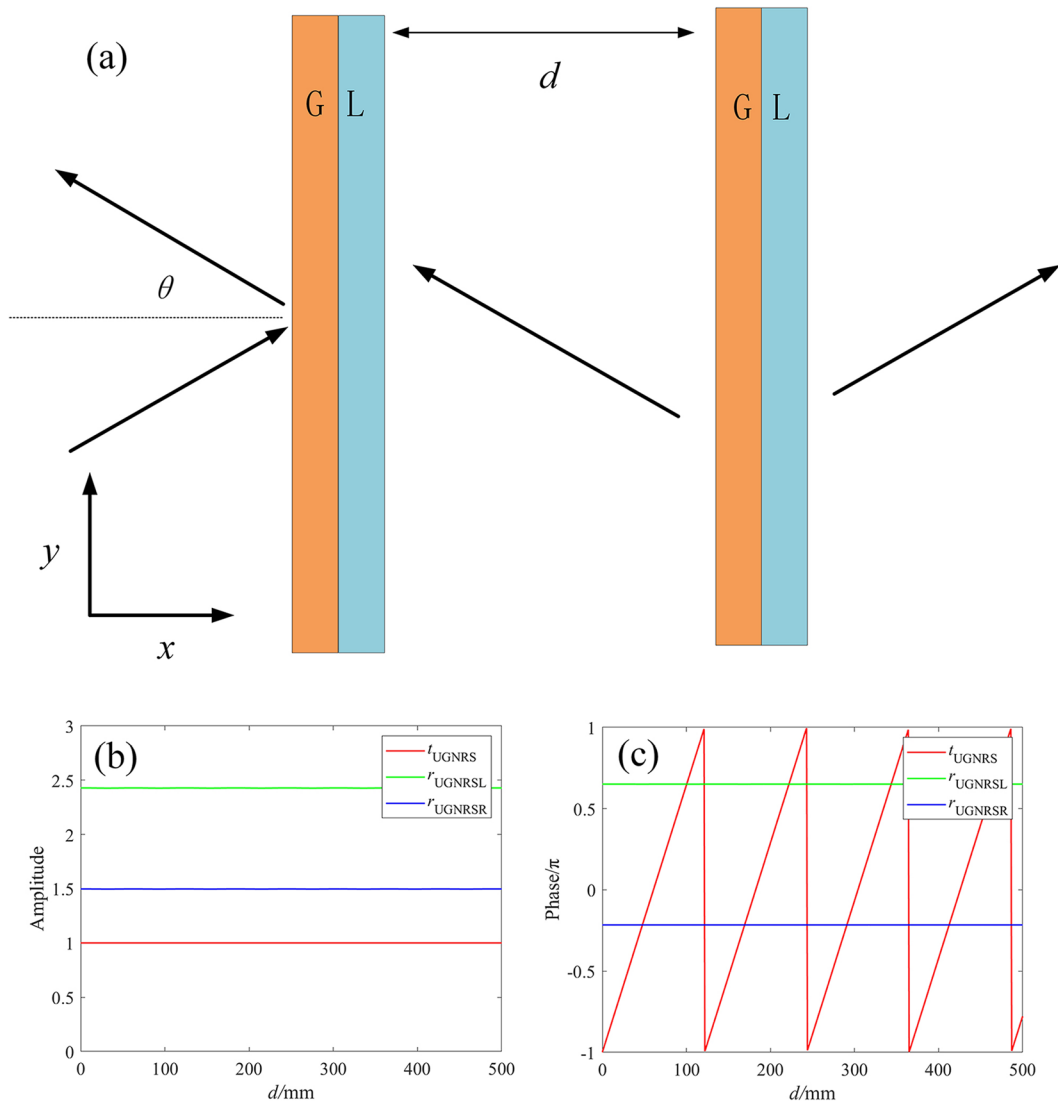


**FIG. 4.** (a) The diagrammatic sketch of the unbalanced gain–loss negative refraction system (UGNRS). The amplitudes and phases of transmission, left-reflection, and right-reflection coefficients of the UGNRS with normally incident wave at 2820 Hz are in (b) and (c), respectively.

plane wave incident from the left and right sides, respectively, can be calculated as

$$P_{mL} = \begin{pmatrix} T_{11} & T_{12} \\ -\frac{1}{T_{12}} & 0 \end{pmatrix} \begin{pmatrix} p_i \\ -\frac{T_{11}}{T_{12}} p_i \end{pmatrix} = \begin{pmatrix} 0 \\ -\frac{1}{T_{12}} p_i \end{pmatrix}, \quad (5)$$

$$P_{mR} = \begin{pmatrix} T_{11} & \frac{1}{T_{12}} \\ -T_{12} & 0 \end{pmatrix} \begin{pmatrix} p_i \\ -T_{11} T_{12} p_i \end{pmatrix} = \begin{pmatrix} 0 \\ -T_{12} p_i \end{pmatrix}. \quad (6)$$

Equations (5) and (6) clearly show that the amplitudes of the forward propagating waves are almost zero incident from both left and right,

and only the backward propagating ones exist. As shown in Figs. 5(a) and 5(d), there are only backward propagations of sound waves between the two surfaces. This indicates the potential of negative refraction of the system.

For oblique incidence, the density should be revised as  $\rho_{G(L)}(\theta) = \rho_{G(L)}/\cos \theta$  and  $c_{G(L)}(\theta) = c_{G(L)} \cos \theta_{G(L)}$  with the change of incident angle  $\theta$  to keep the system working, where  $\theta_{G(L)}$  denotes the complex propagating angle in the gain (loss) region. For  $\theta = 35^\circ$  and  $55^\circ$ , the sound pressure field distributions calculated numerically by using FEM software COMSOL Multiphysics are shown in Figs. 5(b), 5(e), 5(c), and 5(f). The red and white arrows in these pictures denote the different propagation directions of the sound in each area incident from the left side and right side, respectively. The

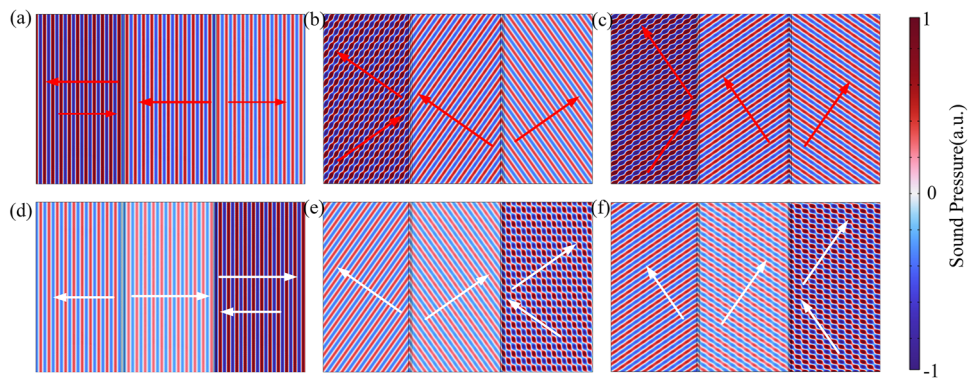


**FIG. 5.** The sound pressure distributions of a plane wave at the frequency of 2820 Hz incident on the UGNRS at the incident angle of (a) and (d)  $0^\circ$ , (b) and (e)  $35^\circ$ , and (c) and (f)  $55^\circ$ . The wave is incident from the left side in (a)–(c) and right side in (d)–(f).

vanish of the forward propagating wave can be observed in both of the incident directions and with different incident angles, showing the bidirectional negative refraction capability of the UGNRS.

## 2. Focusing and imaging

The ability of negative refraction with different angles of the UGNRS inspires us to design a negative refraction focusing and imaging system, i.e., a kind of metasurface. As shown in Fig. 6, a harmonic monopole source at the saser point is placed at a distance of  $o$  from the system ( $o < d$ ), and the sound rays are focused again at two different points, forming two real images, both at a distance  $i = d - o$  from the right surface based on the geometric relationship. The incident angle should be put as  $\theta = \tan^{-1}(y/o)$  in this case depending on the position in the  $y$ -axis of the metasurface, so the parameters of the gain-loss region should be revised correspondingly. According to the calculated results, the negative refraction occurs whether the acoustic wave is incident from left or right, so the focusing and imaging of the system should be bidirectional as well. In Figs. 7(a)–7(d), a 2820 Hz point source is located 625 mm away from the

system in each case, with its source intensity set at  $10^{-3} \text{ m}^2/\text{s}$ , and the distance between the two surfaces is 1250 mm, so the incident angle is  $\theta = \tan^{-1}(2 y/d)$ . It is significant to note that although the transmission direction of the wave when propagating through the metasurface is hardly along the normal direction of the surface, the change in refraction indices and densities in the  $y$  direction of the gain-loss materials has little effect on the propagation because the thickness of the metasurface is only  $2l = 50 \text{ mm} \approx 0.41\lambda_0$ .  $\lambda_0$  is the wavelength of the acoustic wave with the frequency of 2820 Hz in air. From the pictures, we can see two real images emerge at the center of the middle region and the other side in Figs. 7(a) and 7(b) as we predict before. Furthermore, Fig. 7(e) implies the sound intensity on the imaging side along the  $y$  direction at a distance of 625 mm from the surface. This picture shows that the 3 dB beam width is around 60 mm, which is about half the wavelength at the operating frequency, implying a quite high resolution of this imaging system. In addition, Figs. 7(c) and 7(d) show that the system works well in focusing and imaging at the frequency of 2550 and 3450 Hz, respectively, despite being designed at the saser point, which demonstrates the stability of this device.

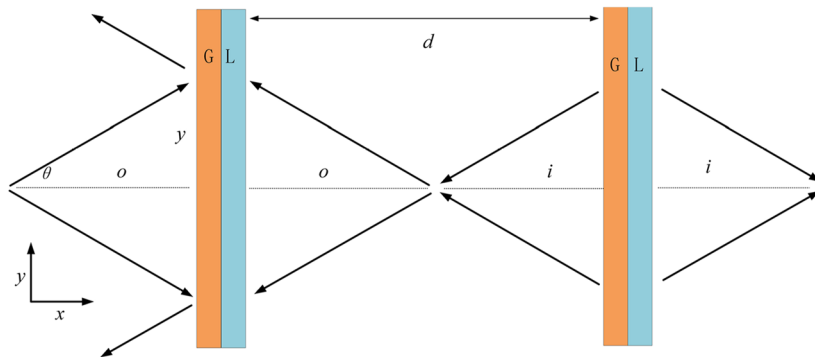


**FIG. 6.** Schematic presentation of the proposed negative refraction focusing system. The monopole source is located on the left side of the focusing system.  $o$  and  $i$  represent the object distance and the image distance, respectively.

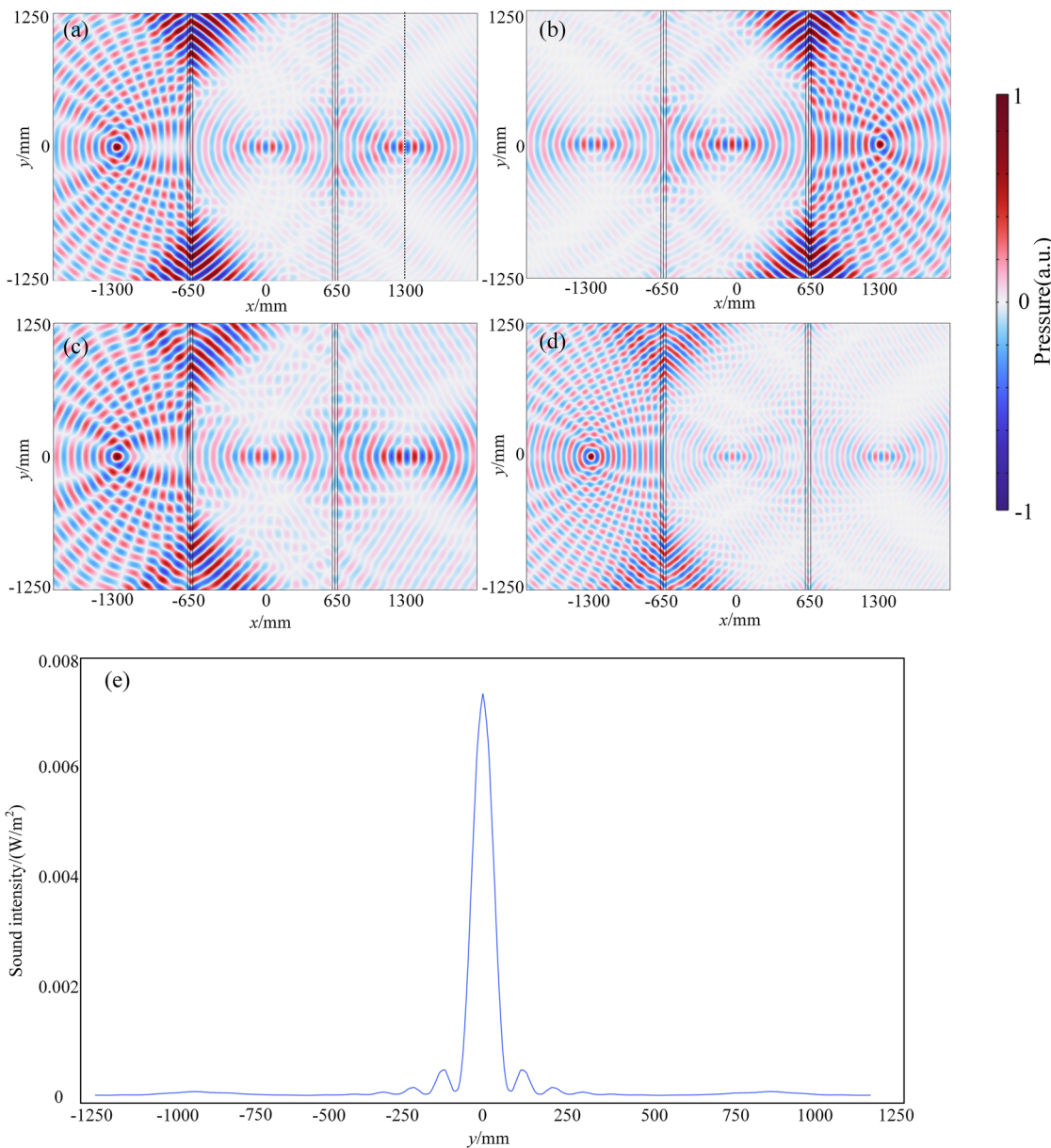


**FIG. 7.** Sound pressure field distributions of the proposed the UGNRS lens (a) and (b) for the frequency of 2820 Hz with the source on the left and right sides, separately, (c) for 2550 Hz, and (d) for 3450 Hz. The distances between the two surfaces are all 1250 mm. The distances from the point sources to the left surfaces in (a), (c), and (d) and the distance from the source to the right surface in (b) are all 625 mm. (e) The sound intensity distribution along the dashed line in (a).

### III. DISCUSSION AND CONCLUSION

In conclusion, we theoretically and numerically investigate an unbalanced gain-loss system. A single metasurface made of a pair of the unbalanced gain-loss regions can produce an extremely high amplification on both the reflectance and transmittance simultaneously at its saser point, which provides a new approach to detecting single frequency acoustic signal and sensitive sensor for surrounding medium besides amplifying the energy of incident wave. Then, the

unbalanced gain-loss negative refraction system based on two parallel metasurfaces is studied, which can act as a metalens achieving bidirectional negative refraction and planar focusing.

The negative refraction system based on parity-time symmetric metasurfaces has been studied before.<sup>29,30,32</sup> For a PT-symmetric negative refraction system with the same geometric design as the unbalanced gain-loss saser system in this work, whose refractive indices are  $n_{G(L)} = 1 \pm 0.585i$ , we calculate the properties by using

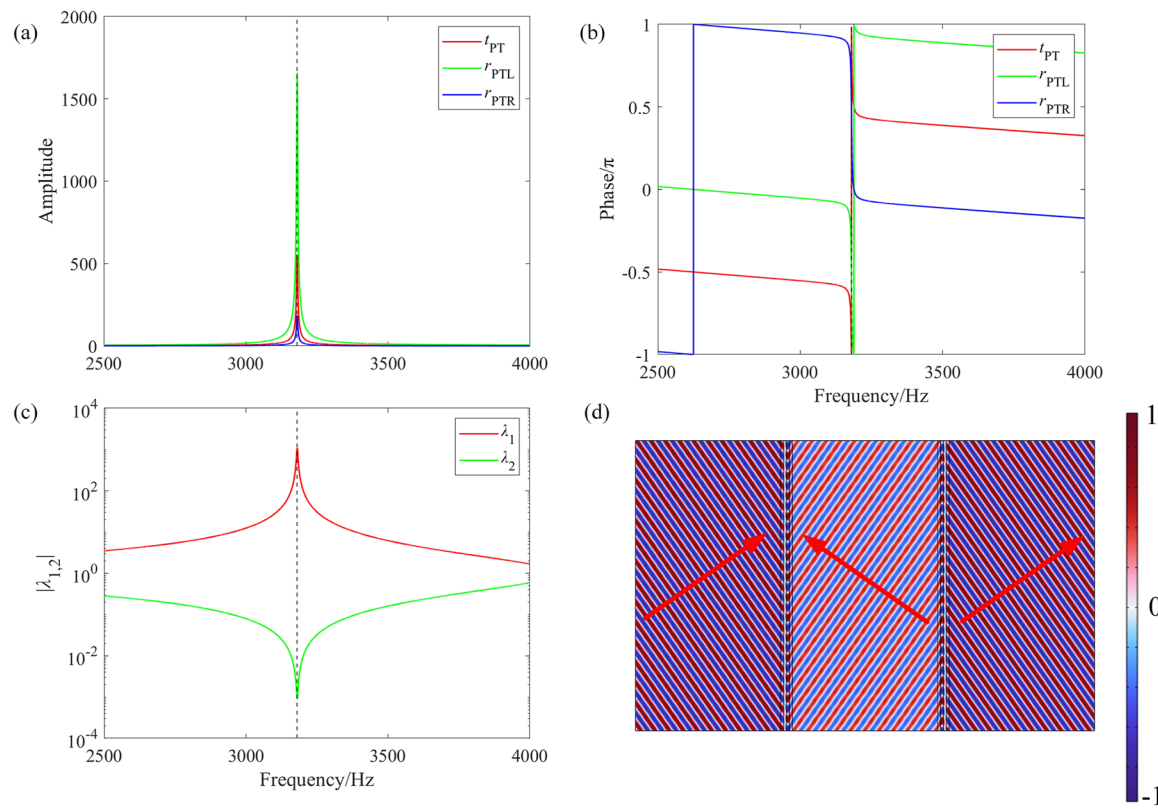


**FIG. 8.** (a) and (b) The amplitude and phase of the transmission, left-reflection, and right-reflection coefficients of the PT-symmetric CPA-saser system with the variation of frequency. (c) The absolute values of the eigenvalues of the scattering matrix of this PT-symmetric system with the variation of frequency. (d) The sound pressure distributions of a plane wave at the frequency of 3180 Hz incident on the PT-symmetric negative refraction system at the incident angle of 35°.

the TMM as well, and the amplitudes and phases of transmission, left-reflection, and right-reflection coefficients of the PT-symmetric CPA-saser system and the eigenvalues of its scattering matrix are in Figs. 8(a)–8(c), respectively. Comparing the two different designs, we find that the system comes to a CPA point ( $|\lambda| = 0$ ) when approaching the saser point (in this case, 3180 Hz) in the PT-symmetric system but there is no CPA point in an unbalanced gain-loss saser system. For the transfer matrix of a PT-symmetric system, the element  $T_{11}$  is always equal to  $T_{22}$ , which indicates that at its CPA-saser point,  $T_{11} = T_{22} = 0$ . Therefore, the reflection of the PT-symmetric negative refraction system with the same design in Fig. 4(a) vanishes based on Eq. (4), and results of numerical simulation in Fig. 8(d) prove it. Although leading to reflection loss, the design of the unbalanced gain-loss system provides a much more flexible approach to negative refraction because for a specific frequency, the saser effect may not occur in the PT-symmetric system. For instance, at the frequency of 2820 Hz, there cannot be saser effect in a PT-symmetric system according to Fig. 2. The results of this work show the potential of the gain-loss system, even unbalanced, of a new kind of multifunctional metamaterial.

## ACKNOWLEDGMENTS

This work was supported by the National Key R & D Program of China (Grant No. 2020YFA0211400), the State Key

Program of National Natural Science of China (Grant No. 11834008), the National Science Foundation of China (Grant No. 12174192), the State Key Laboratory of Acoustics, Chinese Academy of Sciences (Grant No. SKLA202210), the Key Laboratory of Underwater Acoustic Environment, Chinese Academy of Sciences (Grant No. SSHJ-KFKT-1701), the Natural Science Foundation of Jiangsu Province (Grant No. BK20210541), the Natural Science Research of Jiangsu Higher Education Institutions of China (Grant No. 21KJB140003), the Natural Science Foundation of Jiangsu Province (Grant No. BK20210541), and the Natural Science Foundation of the Jiangsu Higher Education Institutions of China (Grant No. 21KJB140003).

## AUTHOR DECLARATIONS

### Conflict of Interest

The authors have no conflicts to disclose.

### Author Contributions

**Zhonghan Fei:** Conceptualization (lead); Data curation (lead); Formal analysis (lead); Investigation (lead); Methodology (equal); Resources (equal); Software (lead); Validation (lead); Writing – original draft (lead); Writing – review & editing (equal). **Jun Lan:**

Conceptualization (supporting); Methodology (equal); Writing – review & editing (equal). **Menyang Gong**: Software (supporting); Writing – review & editing (equal). **Yun Lai**: Writing – review & editing (equal). **Xiaozhou Liu**: Funding acquisition (lead); Supervision (lead); Writing – review & editing (equal).

## DATA AVAILABILITY

The data that support the findings of this study are available from the corresponding author upon reasonable request.

## APPENDIX: THE TRANSFER MATRIX METHOD

The TMM is employed in this paper to get the sound field distribution theoretically. For a normally incident harmonic plane wave, the sound pressure distribution along the  $x$  direction in region A can be expressed as

$$p_{total} = p_+ e^{-jn_A k_0 x} + p_- e^{jn_A k_0 x}, \quad (A1)$$

where the time factor  $e^{j\omega t}$  is omitted.  $\omega = 2\pi f$  ( $f$  is the frequency) is the circular frequency and  $n_A$  is the refractive index of region A, and  $k_0 = \frac{\omega}{c_0}$  is the wave number in air.  $p_+$  and  $p_-$  denote the sound pressure of the wave traveling forward and backward, respectively.

Then, we define a state vector  $P(x) = \begin{pmatrix} p_+ e^{-jn_A k_0 x} \\ p_- e^{jn_A k_0 x} \end{pmatrix}$  for the following calculation. When traveling through a whole region, the vector can be put as  $P(l) = T_A P(0)$ , where the square matrix can be expressed as

$$T_A = \begin{pmatrix} e^{-jn_A k_0 l} & 0 \\ 0 & e^{jn_A k_0 l} \end{pmatrix}. \quad (A2)$$

When the wave propagates through the interface between two regions, for instance, from region A to region B, we have  $P_B(l) = TM_{AB}P_A(l)$ . The square matrix TM is expressed as

$$TM_{AB} = \frac{1}{2} \begin{pmatrix} 1 + \frac{Z_A}{Z_B} & 1 - \frac{Z_A}{Z_B} \\ 1 - \frac{Z_A}{Z_B} & 1 + \frac{Z_A}{Z_B} \end{pmatrix} = TM_{BA}^{-1}, \quad (A3)$$

where  $Z_{A(B)} = \rho_{A(B)} c_{A(B)}$  denotes the characteristic impedance of the materials in the A (B) region, and  $Z_0 = \rho_0 c_0$  is the characteristic impedance of air. The matrix  $TM_{AB(BA)}$ , which denotes the transmission matrix when the wave propagates from the A region to the B region and from the B region to the A region respectively, is determined by the continuance of sound pressure and particle velocity on the interface. Therefore, when a plane wave incident from the left side propagates through the whole structure in Fig. 1, the sound field state vector can be expressed as

$$P_O = \begin{pmatrix} p_t \\ 0 \end{pmatrix} = (TM_{L0} T_L TM_{GL} T_G TM_{0G}) \begin{pmatrix} p_i \\ p_r \end{pmatrix} = T \cdot P_{in}, \quad (A4)$$

$$T = \begin{pmatrix} T_{11} & T_{12} \\ T_{21} & T_{22} \end{pmatrix}. \quad (A5)$$

For oblique incidence, the elements in the transfer matrices varying with the change of the incident angle  $\theta$  can be expressed as

$$T_A(\theta) = \begin{pmatrix} e^{-jn_A(\theta)k_0 d \cos \theta_A} & 0 \\ 0 & e^{jn_A(\theta)k_0 d \cos \theta_A} \end{pmatrix}, \quad (A6)$$

$$TM_{AB}(\theta) = \frac{1}{2} \begin{pmatrix} 1 + \frac{Z_A(\theta)/\cos \theta_A}{Z_B(\theta)/\cos \theta_B} & 1 - \frac{Z_A(\theta)/\cos \theta_A}{Z_B(\theta)/\cos \theta_B} \\ 1 - \frac{Z_A(\theta)/\cos \theta_A}{Z_B(\theta)/\cos \theta_B} & 1 + \frac{Z_A(\theta)/\cos \theta_A}{Z_B(\theta)/\cos \theta_B} \end{pmatrix}, \quad (A7)$$

where  $\theta_A$  and  $\theta_B$  are the complex propagating angle in the A region and B region, respectively, and  $\theta_{A(B)} = \arcsin(\sin \theta / n_{A(B)})$  according to Snell's law. To keep the elements in the transfer matrices of oblique incidence same as the elements in the transfer matrices of normal incidence, and so are the state vectors of sound field distribution, the densities and refractive indices must satisfy

$$n_{A(B)}(\theta) \cos \theta_{A(B)} = n_{A(B)}, \quad (A8)$$

$$Z_{A(B)}(\theta) / \cos \theta_{A(B)} = Z_{A(B)} / \cos \theta. \quad (A9)$$

Thus, the densities and refractive indices will be  $\rho_{A(B)}(\theta) = \rho_{A(B)} / \cos \theta$  and  $n_{A(B)}(\theta) = n_{A(B)} / \cos \theta_{A(B)}$ .

## REFERENCES

- <sup>1</sup>Y. Cheng, J. Xu, and X. Liu, "One-dimensional structured ultrasonic metamaterials with simultaneously negative dynamic density and modulus," *Phys. Rev. B* **77**, 045134 (2008).
- <sup>2</sup>S. H. Lee, C. M. Park, Y. M. Seo, Z. G. Wang, and C. K. Kim, "Composite acoustic medium with simultaneously negative density and modulus," *Phys. Rev. Lett.* **104**, 054301 (2010).
- <sup>3</sup>Y. Cheng, C. Zhou, B. Yuan, D. Wu, Q. Wei, and X. Liu, "Ultra-sparse metasurface for high reflection of low-frequency sound based on artificial Mie resonances," *Nat. Mater.* **14**, 1013–1019 (2015).
- <sup>4</sup>Z. Gu, T. Liu, H. Gao, S. Liang, S. An, and J. Zhu, "Acoustic coherent perfect absorber and laser modes via the non-Hermitian dopant in the zero index metamaterials," *J. Appl. Phys.* **129**, 234901 (2021).
- <sup>5</sup>Q. Wei, Y. Cheng, and X.-j. Liu, "Acoustic total transmission and total reflection in zero-index metamaterials with defects," *Appl. Phys. Lett.* **102**, 174104 (2013).
- <sup>6</sup>H. Chen and C. T. Chan, "Acoustic cloaking in three dimensions using acoustic metamaterials," *Appl. Phys. Lett.* **91**, 183518 (2007).
- <sup>7</sup>P. Chen, M. R. Haberman, and O. Ghattas, "Optimal design of acoustic metamaterial cloaks under uncertainty," *J. Comput. Phys.* **431**, 110114 (2021).
- <sup>8</sup>B. Assouar, B. Liang, Y. Wu, Y. Li, J.-C. Cheng, and Y. Jing, "Acoustic metasurfaces," *Nat. Rev. Mater.* **3**, 460–472 (2018).
- <sup>9</sup>Y. Zhu, X. Fan, B. Liang, J. Cheng, and Y. Jing, "Ultrathin acoustic metasurface-based Schroeder diffuser," *Phys. Rev. X* **7**, 021034 (2017).
- <sup>10</sup>Y. Li and B. M. Assouar, "Acoustic metasurface-based perfect absorber with deep subwavelength thickness," *Appl. Phys. Lett.* **108**, 063502 (2016).
- <sup>11</sup>Y. Zhu, K. Donda, S. Fan, L. Cao, and B. Assouar, "Broadband ultra-thin acoustic metasurface absorber with coiled structure," *Appl. Phys. Express* **12**, 114002 (2019).
- <sup>12</sup>K. Donda, Y. Zhu, S.-W. Fan, L. Cao, Y. Li, and B. Assouar, "Extreme low-frequency ultrathin acoustic absorbing metasurface," *Appl. Phys. Lett.* **115**, 173506 (2019).
- <sup>13</sup>Y. Zhu, A. Merkel, K. Donda, S. Fan, L. Cao, and B. Assouar, "Nonlocal acoustic metasurface for ultrabroadband sound absorption," *Phys. Rev. B* **103**, 064102 (2021).

- <sup>14</sup>C. Zhang, W. K. Cao, L. T. Wu, J. C. Ke, Y. Jing, T. J. Cui, and Q. Cheng, "A reconfigurable active acoustic metasensor," *Appl. Phys. Lett.* **118**, 133502 (2021).
- <sup>15</sup>S. Tang, B. Ren, Y. Feng, J. Song, and Y. Jiang, "Broadband acoustic focusing via binary rectangular cavity/Helmholtz resonator metasurface," *J. Appl. Phys.* **129**, 155307 (2021).
- <sup>16</sup>F. Zhang, E. Perkins, S. Wang, G. T. Flowers, and R. N. Dean, "Compact acoustic metasensor with sinusoidal sub-channels for directional far-field sound beams," *Appl. Phys. Express* **12**, 087002 (2019).
- <sup>17</sup>D.-C. Chen, X.-F. Zhu, D.-J. Wu, and X.-J. Liu, "Broadband airy-like beams by coded acoustic metasurfaces," *Appl. Phys. Lett.* **114**, 053504 (2019).
- <sup>18</sup>H. Gao, Z. Gu, S. Liang, S. An, T. Liu, and J. Zhu, "Coding metasurface for Talbot sound amplification," *Phys. Rev. Appl.* **14**, 054067 (2020).
- <sup>19</sup>X. Fang, X. Wang, and Y. Li, "Acoustic splitting and bending with compact coding metasurfaces," *Phys. Rev. Appl.* **11**, 064033 (2019).
- <sup>20</sup>W. Li, F. Meng, and X. Huang, "Coding metasensor with helical-structured units for acoustic focusing and splitting," *Appl. Phys. Lett.* **117**, 021901 (2020).
- <sup>21</sup>K. Li, B. Liang, J. Yang, J. Yang, and J.-c. Cheng, "Broadband transmission-type coding metamaterial for wavefront manipulation for airborne sound," *Appl. Phys. Express* **11**, 077301 (2018).
- <sup>22</sup>B. Xie, K. Tang, H. Cheng, Z. Liu, S. Chen, and J. Tian, "Coding acoustic metasurfaces," *Adv. Mater.* **29**, 1603507 (2017).
- <sup>23</sup>X. Zhu, H. Ramezani, C. Shi, J. Zhu, and X. Zhang, "PT-symmetric acoustics," *Phys. Rev. X* **4**, 031042 (2014).
- <sup>24</sup>C. M. Bender and S. Boettcher, "Real spectra in non-Hermitian Hamiltonians having PT symmetry," *Phys. Rev. Lett.* **80**, 5243 (1998).
- <sup>25</sup>R. Fleury, D. Sounas, and A. Alù, "An invisible acoustic sensor based on parity-time symmetry," *Nat. Commun.* **6**, 5905 (2015).
- <sup>26</sup>C. Shi, M. Dubois, Y. Chen, L. Cheng, H. Ramezani, Y. Wang, and X. Zhang, "Accessing the exceptional points of parity-time symmetric acoustics," *Nat. Commun.* **7**, 11110 (2016).
- <sup>27</sup>Y. Yang, H. Jia, Y. Bi, H. Zhao, and J. Yang, "Experimental demonstration of an acoustic asymmetric diffraction grating based on passive parity-time-symmetric medium," *Phys. Rev. Appl.* **12**, 034040 (2019).
- <sup>28</sup>T. Liu, G. Ma, S. Liang, H. Gao, Z. Gu, S. An, and J. Zhu, "Single-sided acoustic beam splitting based on parity-time symmetry," *Phys. Rev. B* **102**, 014306 (2020).
- <sup>29</sup>R. Fleury, D. L. Sounas, and A. Alù, "Negative refraction and planar focusing based on parity-time symmetric metasurfaces," *Phys. Rev. Lett.* **113**, 023903 (2014).
- <sup>30</sup>F. Monticone, C. A. Valagianopoulos, and A. Alù, "Parity-time symmetric nonlocal metasurfaces: All-angle negative refraction and volumetric imaging," *Phys. Rev. X* **6**, 041018 (2016).
- <sup>31</sup>J. Lan, L. Wang, X. Zhang, M. Lu, and X. Liu, "Acoustic multifunctional logic gates and amplifier based on passive parity-time symmetry," *Phys. Rev. Appl.* **13**, 034047 (2020).
- <sup>32</sup>J. Lan, X. Zhang, L. Wang, Y. Lai, and X. Liu, "Bidirectional acoustic negative refraction based on a pair of metasurfaces with both local and global PT-symmetries," *Sci. Rep.* **10**, 10794 (2020).
- <sup>33</sup>D. Zhao, Y. Shen, Y. Zhang, X. Zhu, and L. Yi, "Bound states in one-dimensional acoustic parity-time-symmetric lattices for perfect sensing," *Phys. Lett. A* **380**, 2698–2702 (2016).